A time-shared switching scheme designed for multi-probe scanning tunneling microscope

Jiahao Yan, Jiajun Ma, Aiwei Wang, et al.

View Online

Export Citation

CrossMark

ARTICLES YOU MAY BE INTERESTED IN

Simplified feedback control system for scanning tunneling microscopy
Review of Scientific Instruments **92**, 103705 (2021); https://doi.org/10.1063/5.0064511

Performance analysis and implementation of a scanning tunneling potentiometry setup:
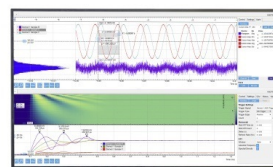Toward low-noise and high-sensitivity measurements of the electrochemical potential
Review of Scientific Instruments **92**, 103707 (2021); https://doi.org/10.1063/5.0064341

A digital feedback system for advanced ion manipulation techniques in Penning traps
Review of Scientific Instruments **92**, 103201 (2021); https://doi.org/10.1063/5.0064369

A time-shared switching scheme designed for multi-probe scanning tunneling microscope

View Online   Export Citation   CrossMark

Jiahao Yan,[1,2] **Jiajun Ma,**[1,2] **Aiwei Wang,**[1,2] **Ruisong Ma,**[1,2] **Liangmei Wu,**[1,2] **Zebin Wu,**[1,2] **Li Liu,**[1,3]
Lihong Bao,[1,4,5] **Qing Huan,**[1,3,4,5,6,a)] **and Hong-Jun Gao**[1,2,4,5,a)]

AFFILIATIONS

[1] Beijing National Laboratory for Condensed Matter Physics and Institute of Physics, Chinese Academy of Sciences, P.O. Box 603, Beijing 100190, China

[2] School of Physical Sciences, University of Chinese Academy of Sciences, Chinese Academy of Sciences, Beijing 100190, China

[3] Jiangxi Institute of Rare Earths, Chinese Academy of Sciences, Ganzhou 341000, China

[4] CAS Center for Excellence in Topological Quantum Computation, University of Chinese Academy of Sciences, Beijing 100190, China

[5] Songshan Lake Materials Laboratory, Dongguan, Guangdong 523808, China

[6] Key Laboratory for Vacuum Physics, University of Chinese Academy of Sciences, Beijing 100190, China

[a)] Authors to whom correspondence should be addressed: huanq@iphy.ac.cn and hjgao@iphy.ac.cn

ABSTRACT

We report the design of a time-shared switching scheme, aiming to realize the manipulation and working modes (imaging mode and transport measurement mode) switching between multiple scanning tunneling microscope (STM) probes one by one with a shared STM control system (STM CS) and an electrical transport characterization system. This scheme comprises three types of switch units, switchable preamplifiers (SWPAs), high voltage amplifiers, and a main control unit. Together with the home-made software kit providing the graphical user interface, this scheme achieves a seamless switching process between different STM probes. Compared with the conventional scheme using multiple independent STM CSs, this scheme possesses more compatibility, flexibility, and expansibility for lower cost. The overall architecture and technique issues are discussed in detail. The performances of the system are demonstrated, including the millimeter scale moving range and atomic scale resolution of a single STM probe, safely approached multiple STM probes beyond the resolution of the optical microscope (1.1 μm), qualified STM imaging, and accurate electrical transport characterization. The combinational technique of imaging and transport characterization is also shown, which is supported by SWPA switches with ultra-high open circuit resistance (909 TΩ). These successful experiments prove the effectiveness and the usefulness of the scheme. In addition, the scheme can be easily upgraded with more different functions and numbers of probe arrays, thus opening a new way to build an extremely integrated and high throughput characterization platform.

Published under an exclusive license by AIP Publishing. https://doi.org/10.1063/5.0056634

I. INTRODUCTION

The scanning tunneling microscope (STM) invented by Binnig *et al.*[1,2] at the beginning of the 1980s lays the foundation of nanotechnology, which has achieved remarkable progress in the past 40 years. In addition, the following various new microscopes collectively known as scanning probe microscopes (SPMs), including atomic force microscope (AFM),[3] scanning tunneling potentiometry (STP),[4–8] and scanning near-field optical microscopy (SNOM),[9,10] enable us to characterize diverse information, such as local electronic structure, magnetic states, molecular vibration,[11] and so on at nanometer-scale. Furthermore, to combine the high spatial resolution features with the electrical transport characterization for low-dimensional materials, multi-probe SPMs, such as double-probe SPM,[12–14] triple-probe SPM,[15,16] and, especially, the quadruple-probe SPM (or four-probe SPM),[17–23] have been developed subsequently.[24,25] Notably, the quadruple-probe SPM can eliminate the ambiguous contact resistance. With these powerful

microscopy systems, a great deal of nanosystems, such as nanowires,[26–28] 2D materials,[29–33] and surface state of 3D materials,[34–37] have been investigated.

The multi-probe SPM system adopted in this work has recently been upgraded[38] from one of the earliest commercial and prototypical four-probe STM systems. Some research works carried out on this system in terms of defect-induced (strain, boundary, and impurity, etc.) electronic and electrical properties of nanowires[18,27] and membranes[30,32,33,39–46] were reported.

To achieve simultaneous operation and imaging by using multiple STM probes, each STM probe needs to be driven by an individual feedback loop, i.e., a whole set of the STM control system (STM CS). However, as the STM probe quantity or piezotube quantity increases, the complexity and cost will increase dramatically. In fact, simultaneous manipulation and imaging via more than one STM probe are quite rare due to crosstalk and cumbersome steps during operations. In this paper, the scheme proposes a home-designed switching circuit and software and fulfills manipulation, imaging, and switching of four STM probes with eight piezotubes via sharing the single STM CS and electrical transport characterization system

(ETCS). Regarding seamless switching, several key technical issues are figured out and discussed, such as jitter elimination of the tip due to the absence of transient driven voltage applied to the piezotube and extremely weak current switching. Eventually, we have succeeded in manipulating the single STM probe at atomic scale with a millimeter scale moving range, approaching multiple STM probes down to tip curvature radius and carrying out STM imaging and electrical transport characterization *in situ*. This time-shared scheme exhibits precise positioning for each STM probe at nanoscale and can realize different modes switching between STM probes. Detailed descriptions of the scheme and performance tests are shown in the following parts.

II. SYSTEM DESIGN

A. Overview

The key point of the scheme, i.e., the time-shared switching system (SS), shown in Fig. 1(a) is managing various types of signal connections, marked by different colors, between multiple STM probes,
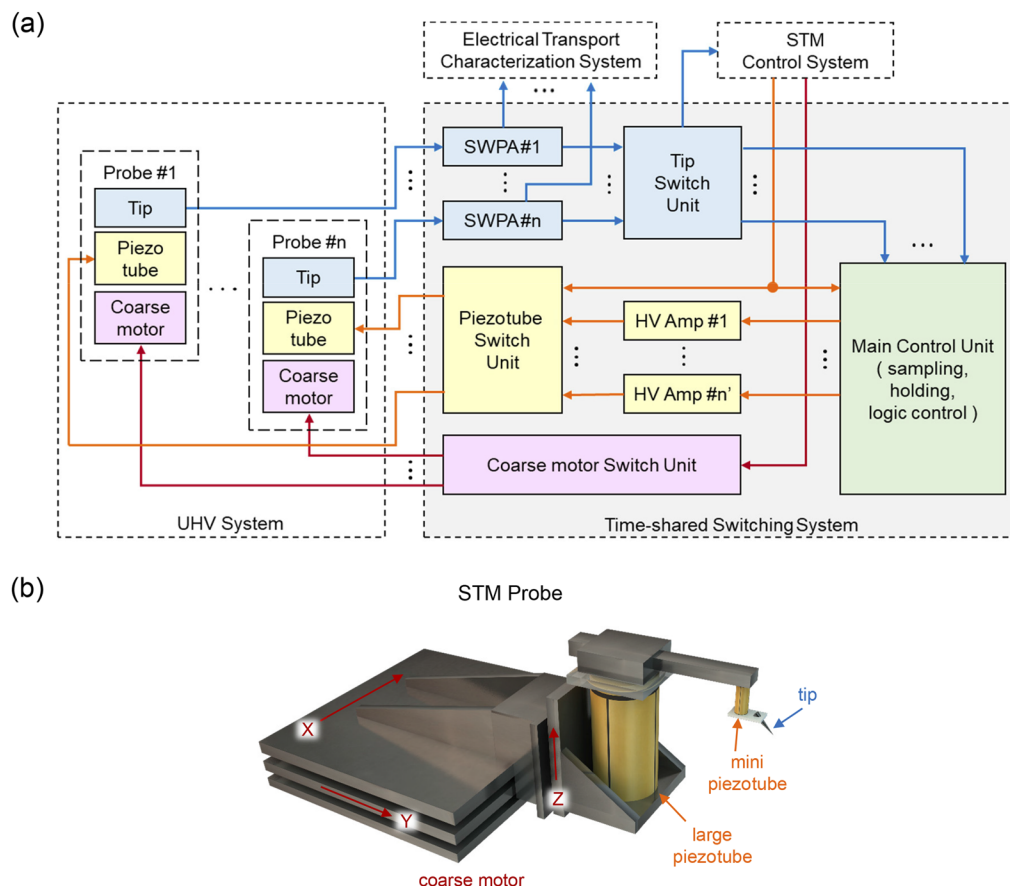

FIG. 1. An overview of the time-shared switching scheme. (a) Schematic illustration of how the time-shared switching system (SS) manages the connection of signal lines between multiple STM probes inside the UHV system, STM control system (STM CS), and electrical transport characterization system (ETCS). Different colors of lines with arrows represent different types of signals. (b) 3D model of each STM probe consisting of the tip, piezotube, and coarse motor. The coarse motor moves in steps in three independent directions marked by the red arrows labeled X, Y, and Z.

single STM CS, and ETCS. The time-shared SS is composed of three types of switch units, switchable preamplifiers (SWPAs), high voltage amplifiers (HV Amps), and a main control unit (MCU). The quantities of all modules, such as SWPAs, HV Amps, and switches, can be flexibly adjusted according to practical requirements. It can also easily support dual-piezo-tube mechanism shown in Fig. 1(b).

The term "probe" represents the entirety consisting of the tip, piezotube, and coarse motor for signal switching, which is shown in the ultra-high vacuum (UHV) system [Fig. 1(a)] and 3D model [Fig. 1(b)]. While describing spatial positioning capability, the term "probe" is equivalent to the term "tip." During STM imaging, the tip works for detecting tunneling current, typically ranging from several picoamp to tens of nanoamp, on a conductive sample. However, when electrical transport is characterized, two or more tips should be involved and all tips and sample will be connected to ETCS. During electrical transport measurement, the voltage typically ranges from −200 to +200 V and the current typically ranges from 1 pA to 100 mA. The coarse motor is stimulated by a high voltage pulse source ranging from −400 to +400 V to move in steps or is grounded when it is idle. The piezotube is driven by slowly varying the high voltage source for providing atomic scale resolution. If the piezotube disconnects from its driven source, it will return to the undeformed state, which leads the tip to unknown position or even tip crashing.

Therefore, the different features and requirements of electrical signals connecting to tips, piezotubes, and coarse motors lead to variations of switching processes and practical circuits. To switch the high dynamic range and sensitive signal connecting to the tip, down to picoamps and up to 100 V in terms of two working modes, it is critical to limit the leak current. Switches with ultra-high open circuit resistance, just placed at the input port of SWPA, are designed for changing connections of the tip to either the STM CS amplifier or ETCS. In addition, one of the magnified tunneling current signals can be connected to the STM CS via the tip switch unit (TSU). To switch high voltage sources driving piezotubes without jitter, it is necessary to avoid the transient absence of voltage. It requires an extra voltage source, i.e., high voltage amplifier (HV Amp), cooperating with strict operation sequence: (1) the HV Amp output identical voltage, (2) connect the HV Amp to the piezotube, and (3) disconnect the STM CS voltage source from the piezotube. A protection resistance is also introduced here for limiting high current flow between the outputs of the STM CS and the HV Amp in case a small voltage difference is present. Operation sequences 2 and 3 and the protection resistance are fulfilled in the piezotube switch unit (PSU). Given that STM probe No. 1 is located at an appropriate position [Fig. 2(b)], then STM probe No. 2 needs to be relocated via STM CS. Before switching, the MCU shown in Fig. 1(a) can acquire the driven voltage on the piezotube from STM CS and make the HV Amp output identical voltage. Then, obeying the sequence mentioned above, the driven source of the piezotube of STM probe No. 1 can switch from STM CS to HV Amp. At this moment, STM probe No. 1 can be disconnected from STM CS safely, while its current signal is still monitored by MCU. Regarding the switch of the coarse motor, it is much easier to just connect it to the signal ground to avoid picking noise as the antenna inside the coarse motor switch unit (CSU).

On the timeline, a conceptional experiment in Fig. 2 fully explains how to dynamically share the single STM CS. For clarification, components inside the UHV system and time-shared SS are

further simplified here. Changes in necessary components during the process, although more or less interconnected, are indicated by filling with colors. At the beginning, Fig. 2(a) shows the initial state that all electronic instruments are idle and two STM probes are far from the specimen. In Fig. 2(b), via time-shared SS, the STM CS connects to STM probe No. 1 and locates it on the specimen surface. In the third step shown in Fig. 2(c), the position of STM probe No. 1 is maintained by using the time-shared SS and disconnected from the STM CS. Next, in Figs. 2(d) and 2(e), STM probe No. 2 repeats the same operations as probe No. 1. Finally, the tip signals of two probes, shown in Fig. 2(f), are connected to the ETCS by using the time-shared SS for measuring the electrical transport properties of the specimen.

B. Hardware

All home-designed modules inside the time-shared SS in Figs. 1(a) and 2, including SWPA, TSU, PSU, CSU, and MCU, are further illustrated in Fig. 3 via 3D models, digital photographs, and highly simplified schematics. There involve so many details of electronic components' selection, chassis and board layout, mix-signal circuit design, and signal ground treatment, etc., but all these aspects will not be discussed here in order to highlight the most important topics. The MCU takes charge in sampling and outputting low voltage, managing all logic controls, and communicating with the host computer. The SWPAs, TSU, PSU, and CSU are designed for switching signals, connecting to tips, piezotubes, and coarse motors, respectively, between the STM CS, ETCS, HV Amps, and MCU.

The SWPA, which has inner reed relay switches (SANYU TPM 95D-1A14N4) labeled S_α, S_β shown in Fig. 3(d), is designed for switching the tip signal between the STM CS preamplifier and the ETCS. Then, the TSU can connect one SWPA output to the STM CS via closing one of the switches labeled S_1 to S_n [Fig. 3(f)]. Simultaneously, all SWPA outputs are monitored by using the MCU through the electronic followers labeled F_1 to F_n [Fig. 3(f)]. The SWPA also has an EXT port and switch S_γ for other functions, such as approaching the tip by monitoring the capacitance change. For the sake of minimizing the leak current, reed switches with ultra-high open circuit resistance are selected and all the signal wires before being fed into the Amp board in Fig. 3(d) are erected in a suspended way, which is indicated within the red box in Fig. 3(b).

The PSU is designed for switching signals connecting piezotubes between the STM CS and the HV Amps. For example, piezotube No. 1 shown in Fig. 3(e) is being manipulated by using the STM CS if switch S_α on board M_1 (M_1-S_α) and switch B_1-S_α inside the PSU are closed. To avoid leading the tip to an unknown position, HV Amp No. 1 needs to supply identical voltage to piezotube No. 1. Moreover, before opening the switch B_1-S_α to make the STM CS idle, the switch B_1-S_β must be closed stably. Otherwise, transient tip jitter will occur. In addition, the resistor on boards B_1 [Fig. 3(e)] is designed for limiting the electrical current.

Compared with the PSU, the CSU is much simpler, and it connects one coarse motor to the STM CS at a time by turning the corresponding switch to state α [Fig. 3(h)]. To avoid introducing noise, all single pole double throw (SPDT) switches marked by S_1 to S_n shown in Fig. 3(h) are at state β to ground all coarse motors by default.
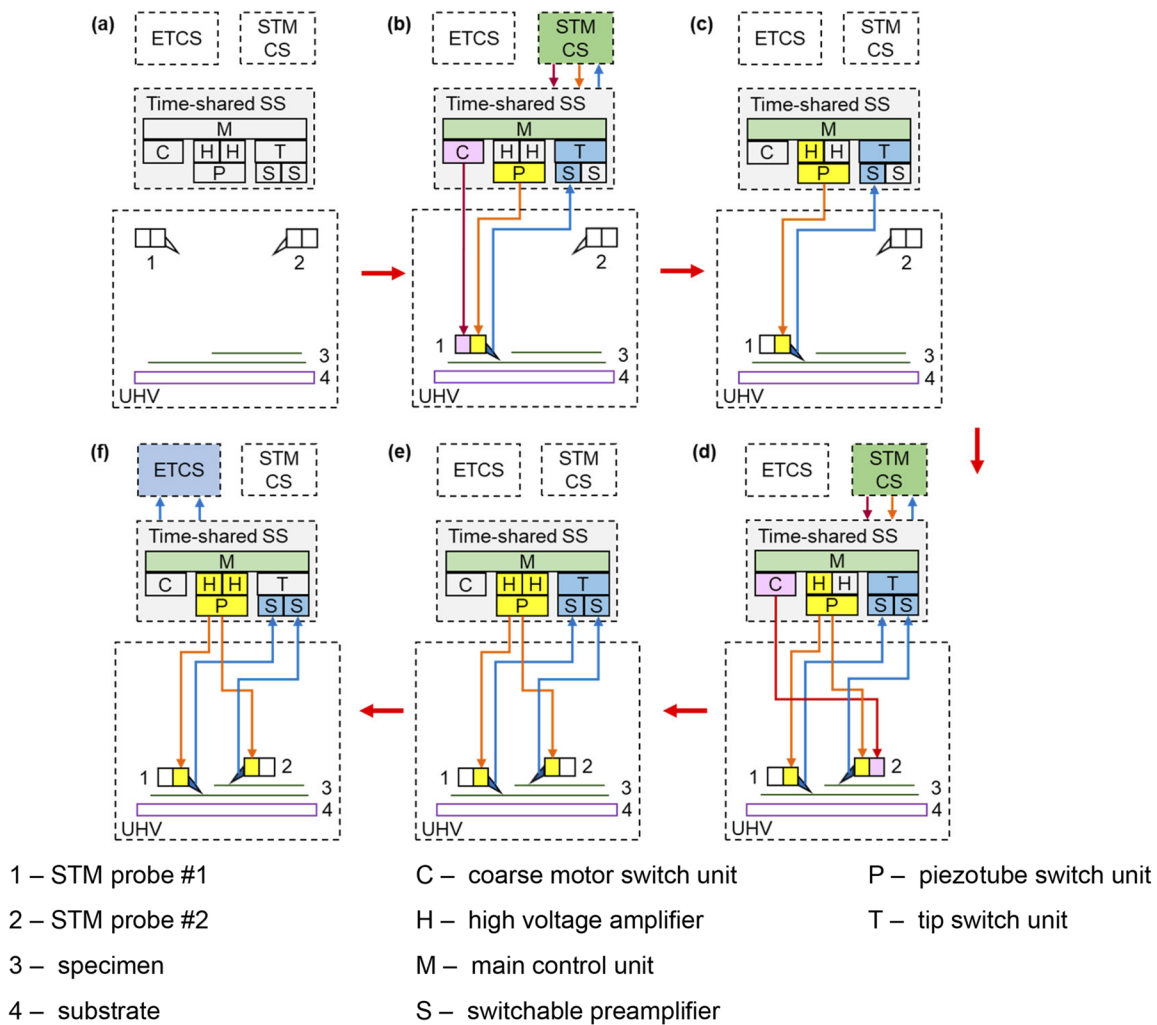
FIG. 2. A conceptional experiment fully explaining how to share the single STM CS on the timeline. (a) Initial state. (b) Location of STM probe No. 1 onto the specimen surface via STM CS and time-shared SS. (c) Position maintenance of probe No. 1 via time-shared SS for setting the STM CS free. [(d) and (e)] Repetition of the same operation on STM probe No. 2 as probe No. 1. (f) Electrical transport property measurement of the specimen after time-shared SS connecting two tips of STM probes to ETCS.

The MCU is designed for controlling all switches, acquiring the voltage value of piezotubes driven by the STM CS via switch M_1-S_β in PSU [Fig. 3(e)], outputting identical voltage to corresponding piezotubes via HV Amp and communicating with the host computer. To realize these complex functions, several different circuit boards partially labeled P_1, A_1, and D_1 are shown in Figs. 3(c) and 3(g). These boards involve the microprocessors, field programmable gate array (FPGA), analog to digital (A/D) converters, and digital to analog (D/A) converters. The DSP microprocessor concentrates on processing raw data such as digital filtering, and the ARM microprocessor runs a task-oriented application on the embedded operating system. For the case of the four-probe STM system adopting dual-piezotube mechanism utilized in this paper ($m > n$ in Fig. 3), at least 130 switches, 24 independent D/A channels, and seven independent A/D channels are required. Therefore, the FPGA chip is introduced

to work as a co-processor of the microprocessors, directly controlling all types of switches, 16 bits D/A converters, and 18 bits A/D converters in real time. To stably measure or supply voltage, the hardware low pass filter (LPF) shown in Fig. 3(g) is used for signal conditioning before the input of A/D or after the output of D/A converters. Notably, as the microprocessor and FPGA are the bridge between the hardware and software, their specific functions will be further discussed in Sec. II C.

C. Software

Figure 4 illustrates the software architecture of the time-shared SS from the perspective of significant function modules and data flow, marked by blocks and arrows, respectively. Aiming to easily upgrade or integrate more powerful tools later, not only the
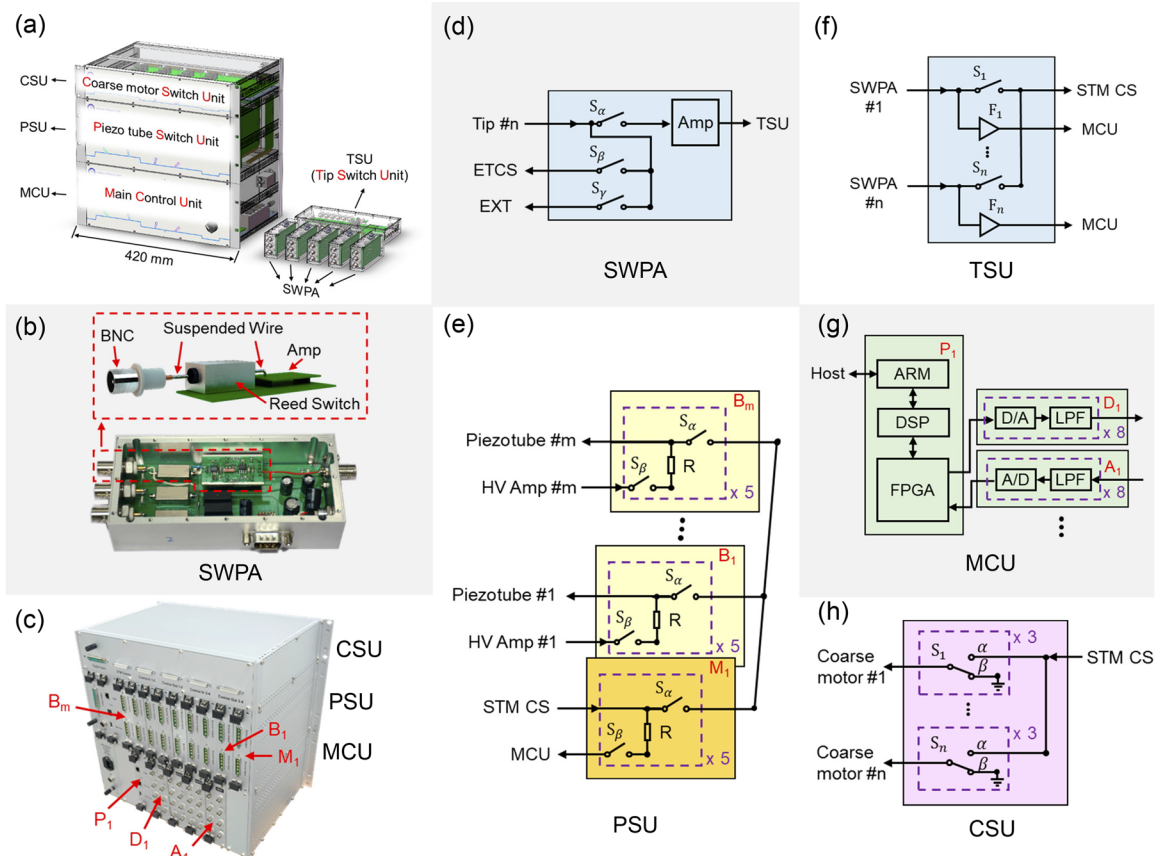
FIG. 3. Hardware design of the time-shared SS in detail. (a) 3D models of the electronic instruments constructing the time-shared SS in front view with a size mark for reference. (b) Digital photograph of the SWPA with inner switches. The 3D model highlighted in the red box shows suspended wires before being fed into the Amp board. (c) Digital photograph of CSU, PSU, and MCU in rear view. [(d)–(h)] Highly simplified schematics of SWPA, PSU, TSU, MCU, and CSU, respectively. The purple dashed boxes multiplied by the number represent the real quantity of the components inside the boxes.
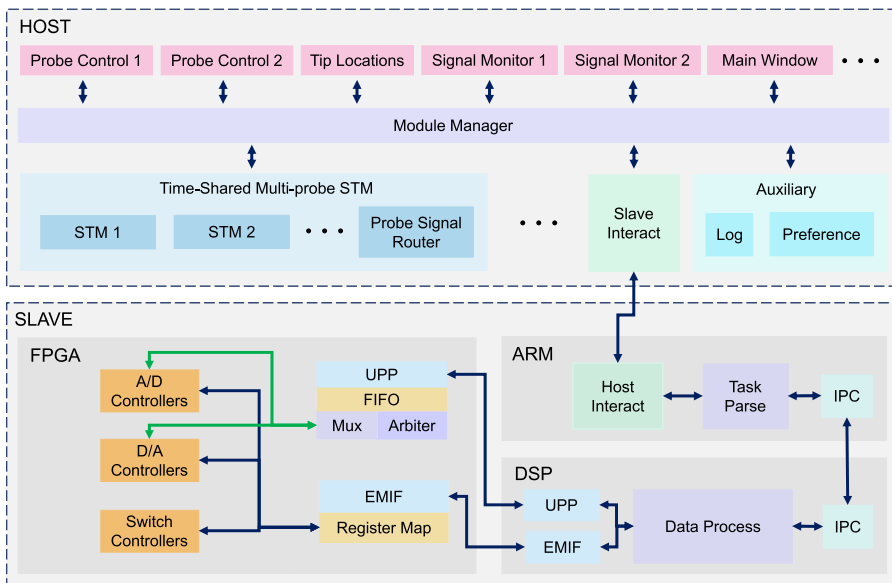

FIG. 4. Software architecture of time-shared SS illustrating the functional modules and data stream represented by arrows interacting between them.

hardware but also the software is designed to adopting an expansible framework via careful division of function modules and uniform definition of data interface. Generally, the software architecture consists of two main parts: host and slave. The host software usually runs on the desktop system of the personal computer, while the slave software runs on the embedded system in MCU. With the software kit offering a graphical user interface (GUI) shown in Fig. 5, merely clicking the mouse will greatly simplify the experimental operations during switching between different STM probes, which must follow strict sequences to control many hardware devices, such as relay switches, D/A converters, and so on.
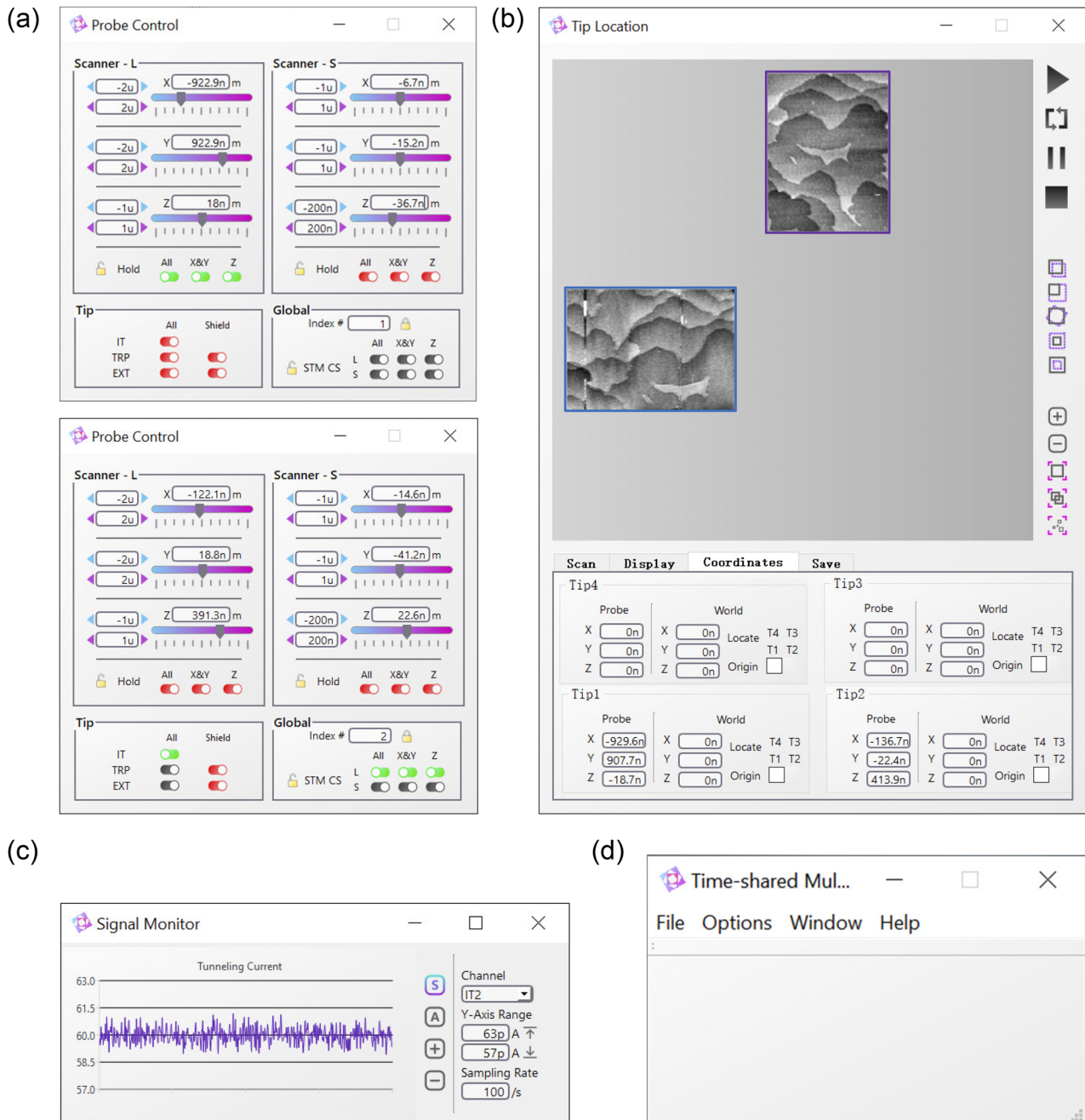

FIG. 5. GUI of time-shared SS showing several significant windows. (a) Panels of probe control responsible for manipulating piezotubes and all switches. (b) Panel of tip location designed for obtaining relative distance of tips according to STM images of the specimen. (c) Panel of the diverse signal monitor. (d) Panel of the main window.

Unlike the slave software orienting data flow, the host software pays much more attention to tasks instead of data flow. A module manager shown in Fig. 4 assigns unique ID numbers to other modules and provides the service of interacting uniform data packets between them. All the pink modules of the host in Fig. 4 labeled by probe control, tip locations, signal monitor, and main window provide corresponding GUI widgets with different functions shown Fig. 5. For example, each probe control widget shown in Fig. 5(a) offers the interactive interface of each independent STM probe, including switches of various signals and an extra voltage source to maintain the tip's position. In addition, the widget named tip locations is presently designed for determining the relative distance between various tips, according to the identical feature of images acquired by using the STM CS from different STM probes. In addition, all the other modules, such as an auxiliary module providing functions of log and preference (Fig. 4), run in the background. As a mapper between the physical level and the hardware level, the time-shared multi-probe STM module instantiates a probe signal router and multiple objects named as STM1, STM2, etc. The former object is responsible for recording and managing the states of all physical relays of the time-shared SS and the latter objects, respectively, describe the corresponding STM probe behaviors and data structures, such as the sensitivity of a piezotube.

If the researcher clicks the widgets on GUI of the host software, such as acquiring voltage values from several A/D converters, corresponding packets will be generated and eventually arrive at the application running on the ARM core, belonging to the slave software via the interaction interface. According to their characteristics, the ARM core, and the DSP core (Fig. 4), interacting data with each other by inter-processor communication (IPC) based on the mechanism of shared memory are in charge of parsing tasks and processing data, such as digital filtering. Then, on the FPGA core shown in Fig. 4, the working state of functional controllers, such as A/D, D/A, and switches, can be changed by the DSP core via writing date of the packet to a specific field of the register map, which can be randomly accessed via an external memory interface (EMIF). Compared with EMIF, the universal parallel port (UPP) without address lines, sequentially accessing to first in first out (FIFO) memory and cooperating with a mux and an arbiter, is much faster and suitable for the conditions transferring massive data, such as multiple A/D converters parallel sampling at high speed in real time. The logic circuit implemented inside the FPGA is designed with Verilog HDL language.

III. PERFORMANCE

To test the performance of the time-shared SS, the electrical specifications, positioning capability of STM probes, STM imaging, and electrical transport characterization are carried out with the Omicron Matrix SPM system and Keithley 4200-SCS at room temperature.

A. Electrical performance

Two tests are discussed here in terms of open circuit resistance of the SWPA switch and long-term stability of the voltage source. As three switches are placed just at the input of SWPA, they can introduce extra leak current to the STM preamplifiers. If the extra leak current increases as much as the signal current during STM imaging or electrical transport characterization, it will affect imaging quality and transport characterization accuracy. Hence, it is necessary to test the open circuit resistance of the SWPA switch. We employ a direct method to do the test. By applying a 100 V voltage across the SWPA switch pins, there is a R–C charging process shown in Fig. 6(a). The R and C here are the resistance and capacitance between switch electrodes and the coil, which are electrically isolated and account for the charging time up to tens of second. The R–C charging process for all other distributed capacitance and wire resistance (<1 Ω) is too short to be detected by Keithley 4200 SCS possessing only millisecond time resolution. The experimental data in Fig. 6(a) can be fitted well by the following equation: $i = i_0 + A(e^{-\frac{t}{\tau}})$. Here, i_0 representing the leak current is equal to 110 fA, which is much smaller than the normal working value. In addition, the open circuit resistance of the switch can be up to 909 TΩ. Compared with the coaxial cable, the capacitance of SWPA is negligible.

Usually, most tips are required to be held at the known position for quite a long time, e.g., the rest tips not doing STM imaging or the tips measuring electrical transport properties. Hence, the output value of the low voltage source to maintain the piezotube position, via HV Amp, must be constant. Figure 6(b) shows the stability of the low voltage source, which fluctuates within 0.06 mV for 12 h. Compared with the tip drift caused by temperature (24 nm/h),[38] the drift due to voltage source fluctuation is negligible (<0.01 nm/12 h, supposing that HV Amp gain is 15 and piezotube sensitivity is 10 nm/V). The alternating current (AC) noise can be greatly reduced by the R–C filter, which consists of protection resistance with a larger value shown in Fig. 3(e) and piezotube capacitance.
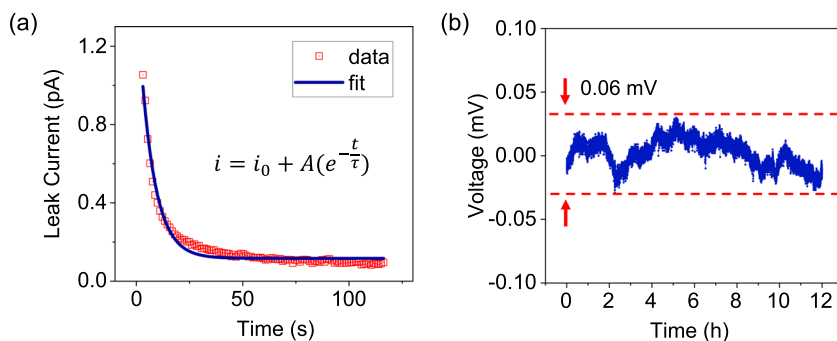

FIG. 6. Electrical performance of significant components in the time-shared SS. (a) Leak current of the reed switch inside the SWPA. The red square dots represent data, and the blue line represents the fitting curve. (b) Stability of the low voltage source measured at 1 V during 12 h for maintaining the tip's position. The data are offset to clearly show the fluctuation.

B. Performance of single STM probe

Owing to adoption of dual-piezotubes' mechanism in the upgraded system shown in Fig. 1(b), the tip position of each STM probe is determined together by using the two piezotubes. Compared with the mini piezotube, the large piezotube with much longer cantilever can hardly obtain an atomic image. Therefore, the seamless switching between two different piezotubes for a single STM probe by using the time-shared SS is demonstrated here. Figure 7(b) obtained by using the large piezotube shows the topography of the area in the optical image marked by the blue dot around the tip apex in Fig. 7(a). After maintaining the large piezotube by using the time-shared SS at the center of the red squared box [Fig. 7(b)], the STM CS manipulates the mini piezotube to obtain a clear structure of this area [Fig. 7(c)]. Then, the atomic image shown in Fig. 7(d) of the area marked by the red box in Fig. 7(c) can also be obtained. As a result, the tip status is unchanged and there is no distinct image shift after switching. In addition, by combining the performance of a powerful OM (millimeter scale: 1.1 μm), large piezotube (nanoscale: 4 μm), and mini piezotube (atomic scale: 400 nm) shown in Fig. 7, the system possesses atomic scale resolution and the millimeter scale probing range.

C. Positioning multiple STM probes

The reliable collaborations among multiple STM probes are demonstrated here. First, the nearest distance between two tips achieved is the question of the most concern. Figure 8(a) shows two slant tips approaching each other over the sample under the guidance of an OM. However, under the OM, the closest distance is limited by the OM resolution, as shown in Fig. 8(b). Further decreasing the tips' distance relies on STM imaging capability. If identical features can be found in two STM images obtained by two neighboring tips, then that means the two scan areas overlap, as illustrated in Fig. 8(d). Then, the horizontal distance between apexes of two slant tips marked by d shown in Fig. 8(a) can be determined. Figures 8(e) and 8(f) show the STM images obtained by two tips on the Au (111) surface containing identical features highlighted. Accordingly, these

two tips' distance d is 1133 nm. The nearest distance is determined by the curvature radius of tip apexes. For instance, Fig. 8(c) shows the image obtained from tip1, which encountered tip2 at the bottom area, indicating that both tips' apex radii are less than 150 nm.

Similarly, an approaching process with three or more tips is illustrated in Fig. 9. In this case, a larger area of the overlapping shadow in the optical view [Fig. 9(a)] impedes the process of finding identical features in STM images. Therefore, a much safer method, with the known distance between tips before they approach to each other, is proposed. With the help of coarse motors, multiple horizontal strip areas of the sample scanned by tip3 [green blocks shown in Fig. 9(c)] can form a moving path with enough length for the OM to distinguish [green dashed line with arrow in Fig. 9(b)]. Then, the distance of other tips from tip3 can be obtained, respectively, by overlapping the scan areas shown in Fig. 9(c). In this process, the collision risk between tips is reduced. The highlight areas with the same color in Fig. 9(d) indicate identical features obtained from three tips on the Au (111) surface, respectively. Eventually, the three tips can be further approached to each other shown in Fig. 9(e), according to the result in Fig. 9(d).

D. Imaging and electrical transport characterization

As extra switches are introduced into SWPA, it is imperative to test the system's STM imaging quality and electrical transport characterization accuracy. The clear STM atomic image [Fig. 10(b)] and identical transport curves of graphene sheet obtained [Fig. 10(a)] by the van der Pauw method[47,48] [the inset of Fig. 10(a)] have given a positive answer. Then, combinational technique of STM imaging and electrical transport characterization *in situ* inspired by STP is further discussed due to strong coupling between imaged structure and electrical transport properties at nanoscale.[49,50] STM images of the flat graphite surface and wrinkle [the bottom inset of Figs. 10(e) and 10(f)] can be obtained by tip3 connecting to STM CS, with tip1 and tip2 supplying the same voltage [Fig. 10(c)]. The corresponding height profile near the wrinkle shown in Fig. 10(d) reveals a much larger fluctuation in the range of ~25 nm than that of the flat area
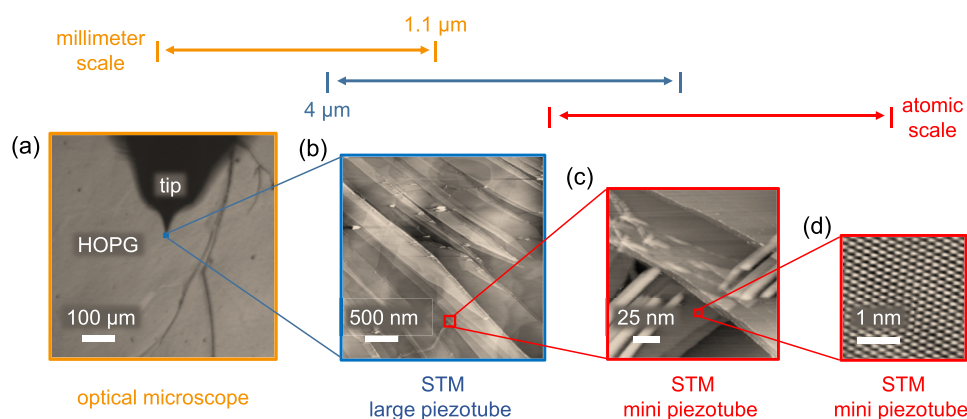

FIG. 7. Atomic scale spatial resolution of a single STM probe with the millimeter scale moving range. (a) Optical image of the tip on the HOPG surface. The scale bar is 100 μm. (b) STM image of the area marked by a blue dot in (a) obtained by using the large piezotube. The scale bar is 500 nm. (c) STM image of the area marked by a red box in (b) obtained by using the mini piezotube. The scale bar is 25 nm. (d) Atomic image of the area marked by a red box in (c) obtained by using the mini piezotube. The scale bar is 1 nm.
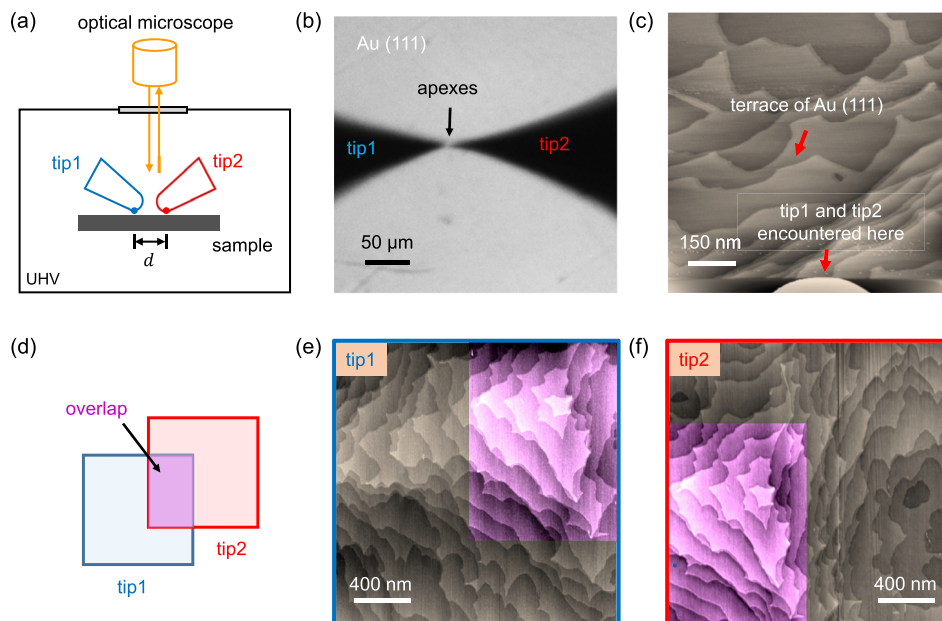
FIG. 8. Approaching two tips ultra-close beyond the spatial resolution limitation of OM. (a) Schematic illustrating how to locate tips in optical scale. (b) Optical image of two approaching tips on the Au (111) surface exhibits unclear and overlapping shadow at apexes. The scale bar is 50 μm. (c) STM image obtained from tip1 within the area containing tip2 on the Au (111) surface. The scale bar is 150 nm. (d) Schematic illustrating the overlap between the scanning areas of two tips for approaching them ultra-close. [(e) and (f)] STM topographic images of Au (111) with highlighted identical features, respectively, obtained by tip1 and tip2 reveal that their scan areas have overlapped. The scale bar is 400 nm.
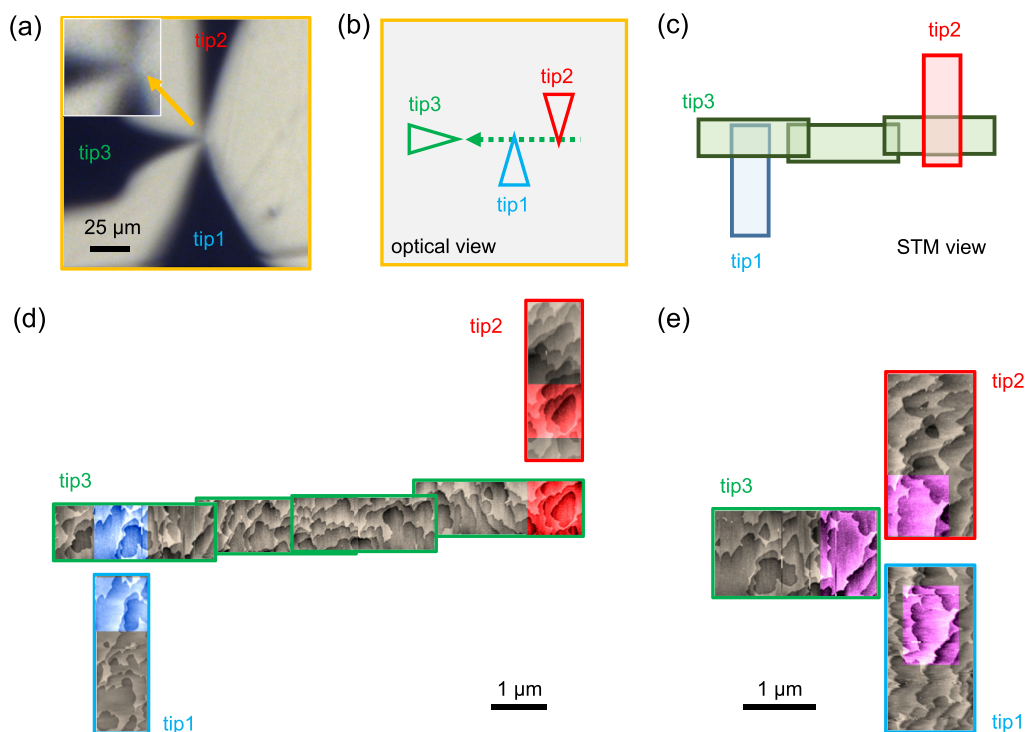

FIG. 9. A safe method to approach three or more tips ultra-close. (a) Optical image of three tips located on the Au (111) surface. The scale bar is 25 μm. Inset: Zoom-in image at apexes shows extremely overlapping shadows. (b) Schematic illustrating the method in optical view. (c) Schematic illustrating the method in STM view corresponding to (b). (d) STM images of Au (111) obtained by three tips. The highlighted blue and red regions show the identical features, respectively. The scale bar is 1 μm. (e) Safely approaching three tips with the known relative distance ultra-close proved by the identical features in highlighted regions. The scale bar is 1 μm.
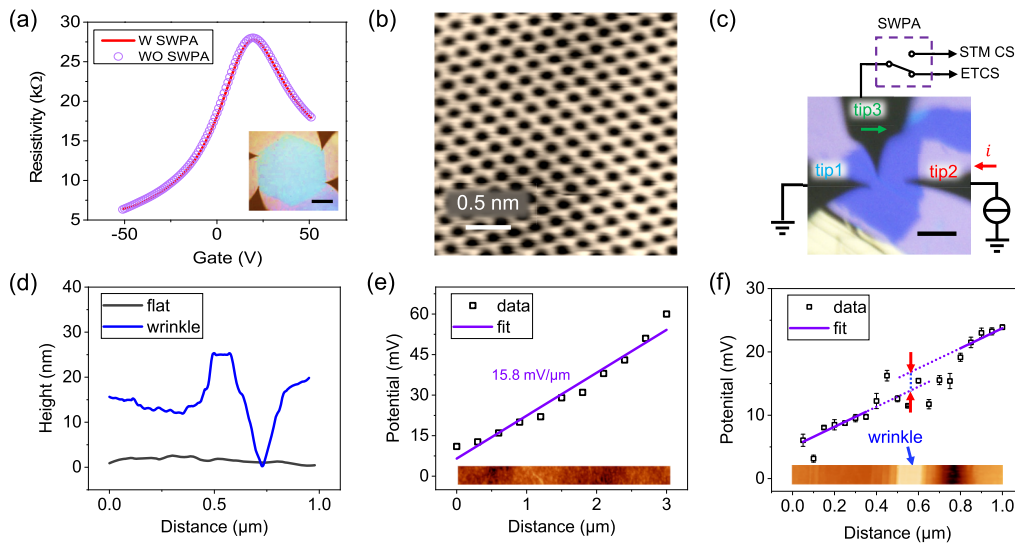
FIG. 10. STM imaging and transport characterization of graphene sheet and graphite wrinkle with two methods, respectively. (a) Measuring the electrical transport properties of the graphene/SiO$_2$ sample with (red line) and without (purple circles) SWPA possessing the inner switch. Inset: Optical image of the sample. The scale bar is 200 μm. (b) Atomic image of graphene in (a). The scale bar is 0.5 nm. (c) Schematic illustrating the experimental setup to investigate influence near wrinkle on the potential distribution of the graphite surface. The scale bar is 300 μm. (d) Height profiles obtained from the STM image of the flat and wrinkle area in bottom of (e) and (f), respectively. [(e) and (f)] Evolution of potential with distance and the STM image of the flat and wrinkle area, respectively. The potential data here are offset to zero for clarity.

(~3 nm). The evolution of electrical potential with distance in the flat area and wrinkle area [square dots in Figs. 10(e) and 10(f)] can be obtained by tip3 connecting to ETCS, with tip1 and tip2 injecting constant current. Neglecting the eight middle dots in Fig. 10(f) oscillating probably due to mechanical instability of wrinkle, the six left dots (except the second one) and five right dots in Fig. 10(f) are, respectively, fitted with equation $y = kx + b$, where k equals the fitted slope in the flat area [15.8 mV/μm in Fig. 10(e)]. Therefore, the influence near the wrinkle area on the graphite surface potential distribution here is 2.92 mV, highlighted by two red arrows in Fig. 10(f), which is the intercept difference of lines fitted above (b_l = 5.02 and b_r = 7.94). The succession in relating imaging and electrical transport by a protype experiment here lays the foundation for exploring the integrated measurement environment with more advanced techniques for the research on low-dimensional material in the future.

IV. CONCLUSIONS

We present the design of a time-shared switching scheme, which enables the single STM CS to manipulate multiple STM probes. Compared with the conventional scheme using multiple independent STM CSs, this scheme possesses more compatibility and expansibility, but with lower cost. The functional modules of our scheme, be it hardware or software, are home designed. To realize seamless switching, a batch of technical difficulties needs to be solved, such as tip jitter elimination and weak current switching. The whole system performance is tested, including single STM probe manipulation at atomic scale with a millimeter scale moving range, multiple STM probes approaching down to tip curvature radius,

qualified STM imaging, and accurate electrical transport characterization. The combinational technique of imaging and transport characterization is supported by SWPA switches with ultra-high open circuit resistance (909 TΩ). We expect that these inspiring results will offer a feasible path for similar multi-probe STM systems and play significant roles in high throughput, intelligent, and automated characterization platform for low-dimensional material research in the future.

DATA AVAILABILITY

The data that support the findings of this study are available from the corresponding authors upon reasonable request.

REFERENCES

[1] G. Binnig and H. Rohrer, Helv. Phys. Acta **55**, 726 (1982).
[2] G. Binning, H. Rohrer, C. Gerber, and E. Weibel, Phys. Rev. Lett. **49**, 57 (1982).
[3] G. Binnig, C. F. Quate, and C. Gerber, Phys. Rev. Lett. **56**, 930 (1986).
[4] A. Bannani, C. A. Bobisch, and R. Möller, Rev. Sci. Instrum. **79**, 083704 (2008).
[5] K. W. Clark, X.-G. Zhang, I. V. Vlassiouk, G. W. He, R. M. Feenstra, and A.-P. Li, ACS Nano **7**, 7956 (2013).

[6] P. Muralt and D. W. Pohl, Appl. Phys. Lett. **48**, 514 (1986).

[7] B. G. Briner, R. M. Feenstra, T. P. Chin, and J. M. Woodall, Phys. Rev. B **54**, R5283 (1996).

[8] K. W. Clark, X. G. Zhang, G. Gu, J. Park, G. W. He, R. M. Feenstra, and A. P. Li, Phys. Rev. X **4**, 011021 (2014).

[9] D. W. Pohl, W. Denk, and M. Lanz, Appl. Phys. Lett. **44**, 651 (1984).

[10] A. Harootunian, E. Betzig, M. Isaacson, and A. Lewis, Appl. Phys. Lett. **49**, 674 (1986).

[11] B. C. Stipe, M. A. Rezaei, and W. Ho, Science **280**, 1732 (1998).

[12] H. Grube, B. C. Harrison, J. F. Jia, and J. J. Boland, Rev. Sci. Instrum. **72**, 4388 (2001).

[13] H. Watanabe, C. Manabe, T. Shigematsu, and M. Shimizu, Appl. Phys. Lett. **78**, 2928 (2001).

[14] E. Tsunemi, K. Kobayashi, K. Matsushige, and H. Yamada, Rev. Sci. Instrum. **82**, 033708 (2011).

[15] H. Watanabe, C. Manabe, T. Shigematsu, K. Shimotani, and M. Shimizu, Appl. Phys. Lett. **79**, 2462 (2001).

[16] M. Salomons, B. V. C. Martins, J. Zikovsky, and R. A. Wolkow, Rev. Sci. Instrum. **85**, 045126 (2014).

[17] I. Shiraki, F. Tanabe, R. Hobara, T. Nagao, and S. Hasegawa, Surf. Sci. **493**, 633 (2001).

[18] X. Lin, X. B. He, J. L. Lu, L. Gao, Q. Huan, D. X. Shi, and H. J. Gao, Chin. Phys. **14**, 1536 (2005).

[19] R. Hobara, N. Nagamura, S. Hasegawa, I. Matsuda, Y. Yamamoto, Y. Miyatake, and T. Nagamura, Rev. Sci. Instrum. **78**, 053705 (2007).

[20] T. H. Kim, Z. H. Wang, J. F. Wendelken, H. H. Weitering, W. Z. Li, and A. P. Li, Rev. Sci. Instrum. **78**, 123701 (2007).

[21] S. Higuchi, H. Kuramochi, O. Laurent, T. Komatsubara, S. Machida, M. Aono, K. Obori, and T. Nakayama, Rev. Sci. Instrum. **81**, 073706 (2010).

[22] S. Higuchi, O. Kubo, H. Kuramochi, M. Aono, and T. Nakayama, Nanotechnology **22**, 285205 (2011).

[23] V. Cherepanov, E. Zubkov, H. Junker, S. Korte, M. Blab, P. Coenen, and B. Voigtländer, Rev. Sci. Instrum. **83**, 033707 (2012).

[24] T. Nakayama, O. Kubo, Y. Shingaya, S. Higuchi, T. Hasegawa, C.-S. Jiang, T. Okuda, Y. Kuwahara, K. Takami, and M. Aono, Adv. Mater. **24**, 1675 (2012).

[25] A.-P. Li, K. W. Clark, X.-G. Zhang, and A. P. Baddorf, Adv. Funct. Mater. **23**, 2509 (2013).

[26] S. Yoshimoto, Y. Murata, K. Kubo, K. Tomita, K. Motoyoshi, T. Kimura, H. Okino, R. Hobara, I. Matsuda, S. Honda, M. Katayama, and S. Hasegawa, Nano Lett. **7**, 956 (2007).

[27] X. Lin, X. B. He, T. Z. Yang, W. Guo, D. X. Shi, H.-J. Gao, D. D. D. Ma, S. T. Lee, F. Liu, and X. C. Xie, Appl. Phys. Lett. **89**, 043103 (2006).

[28] Y. Kitaoka, T. Tono, S. Yoshimoto, T. Hirahara, S. Hasegawa, and T. Ohba, Appl. Phys. Lett. **95**, 052110 (2009).

[29] P. W. Sutter, J.-I. Flege, and E. A. Sutter, Nat. Mater. **7**, 406 (2008).

[30] H. L. Lu, C. D. Zhang, H. M. Guo, H. J. Gao, M. Liu, J. A. Liu, G. Collins, and C. L. Chen, ACS Appl. Mater. Interfaces **2**, 2496 (2010).

[31] M. K. Yakes, D. Gunlycke, J. L. Tedesco, P. M. Campbell, R. L. Myers-Ward, C. R. Eddy, D. K. Gaskill, P. E. Sheehan, and A. R. Laracuente, Nano Lett. **10**, 1559 (2010).

[32] M. Liu, Q. Zou, C. R. Ma, G. Collins, S. B. Mi, C. L. Jia, H. M. Guo, H. J. Gao, and C. L. Chen, ACS Appl. Mater. Interfaces **6**, 8526 (2014).

[33] Q. Zou, M. Liu, G. Q. Wang, H. L. Lu, T. Z. Yang, H. M. Guo, C. R. Ma, X. Xu, M. H. Zhang, J. C. Jiang, E. I. Meletis, Y. Lin, H. J. Gao, and C. L. Chen, ACS Appl. Mater. Interfaces **6**, 6704 (2014).

[34] I. Matsuda, C. Liu, T. Hirahara, M. Ueno, T. Tanikawa, T. Kanagawa, R. Hobara, S. Yamazaki, and S. Hasegawa, Phys. Rev. Lett. **99**, 146805 (2007).

[35] J. C. Li, Y. Wang, and D. C. Ba, Phys. Procedia **32**, 347 (2012).

[36] C. Durand, X. G. Zhang, S. M. Hus, C. X. Ma, M. A. McGuire, Y. Xu, H. L. Cao, I. Miotkowski, Y. P. Chen, and A. P. Li, Nano Lett. **16**, 2213 (2016).

[37] T. Kambe, R. Sakamoto, T. Kusamoto, T. Pal, N. Fukui, K. Hoshiko, T. Shimojima, Z. F. Wang, T. Hirahara, K. Ishizaka, S. Hasegawa, F. Liu, and H. Nishihara, J. Am. Chem. Soc. **136**, 14357 (2014).

[38] R. S. Ma, Q. Huan, L. M. Wu, J. H. Yan, Q. Zou, A. W. Wang, C. A. Bobisch, L. H. Bao, and H. J. Gao, Rev. Sci. Instrum. **88**, 063704 (2017).

[39] Z. W. Shi, H. L. Lu, L. C. Zhang, R. Yang, Y. Wang, D. H. Liu, H. M. Guo, D. X. Shi, H. J. Gao, E. G. Wang, and G. Y. Zhang, Nano Res. **5**, 82 (2012).

[40] J. H. Yan, L. M. Wu, R. S. Ma, S. Y. Zhu, C. Bian, J. J. Ma, Q. Huan, L. H. Bao, J. H. Mao, S. X. Du, and H. J. Gao, 2D Mater. **6**, 045050 (2019).

[41] R. S. Ma, Q. Huan, L. M. Wu, J. H. Yan, W. Guo, Y. Y. Zhang, S. Wang, L. H. Bao, Y. Q. Liu, S. X. Du, S. T. Pantelides, and H. J. Gao, Nano Lett. **17**, 5291 (2017).

[42] R.-S. Ma, Q. Huan, L.-M. Wu, J.-H. Yan, Y.-Y. Zhang, L.-H. Bao, Y.-Q. Liu, S.-X. Du, and H.-J. Gao, Chin. Phys. B **26**, 066801 (2017).

[43] Q. J. Wang, J. H. Yan, M. C. Xiao, D. Manoj, C. Zhong, Q. Y. Lv, L. T. Yang, L. M. Wu, Z. P. Wang, L. H. Bao, H. J. Gao, F. Xiao, L. Jiang, and S. Wang, RSC Adv. **9**, 29327 (2019).

[44] W. Guo, K. Chi, J. H. Yan, L. H. Bao, S. Wang, and Y. Q. Liu, Sci. Bull. **65**, 1356 (2020).

[45] R. S. Ma, J. J. Ma, J. H. Yan, L. M. Wu, H. T. Liu, W. Guo, S. Wang, Q. Huan, X. Lin, L. H. Bao, S. T. Pantelides, and H. J. Gao, 2D Mater. **6**, 045033 (2019).

[46] R. S. Ma, J. J. Ma, J. H. Yan, L. M. Wu, W. Guo, S. Wang, Q. Huan, L. H. Bao, S. T. Pantelides, and H. J. Gao, Nanoscale **12**, 12038 (2020).

[47] L. J. van der Pauw, Philips Tech. Rev. **20**, 220 (1958).

[48] L. J. van der Pauw, Philips Res. Rep. **13**, 1 (1958).

[49] S. Y. Qin, T. H. Kim, Y. N. Zhang, W. J. Ouyang, H. H. Weitering, C. K. Shih, A. P. Baddorf, R. Q. Wu, and A. P. Li, Nano Lett. **12**, 938 (2012).

[50] C. H. Lee, S. Y. Qin, M. A. Savaikar, J. S. Wang, B. Y. Hao, D. Y. Zhang, D. Banyai, J. A. Jaszczak, K. W. Clark, J. C. Idrobo, A. P. Li, and Y. K. Yap, Adv. Mater. **25**, 4544 (2013).